# Failure Characteristics in Thermoplastic Composite Laminates Due to an Eccentric Circular Discontinuity

J. A. Daniels* and A. N. Palazotto†
*Air Force Institute of Technology, Wright-Patterson Air Force Base, Ohio 45433*
and
R. S. Sandhu‡
*Wright Research and Development Center, Wright-Patterson Air Force Base, Ohio 45433*

**Experimental and analytical studies were conducted to observe the failure characteristics of Gr/PEEK specimens containing an eccentric 0.4-in.-diam circular discontinuity. Specimens were loaded in axial tension at room temperature. The stacking sequences considered were $[0\ \text{deg}_{16}]$, $[90\ \text{deg}_{16}]$, $[\pm 45\ \text{deg}]_{4s}$, and $[0/\pm 45/90]_{2s}$. For each stacking sequence, three values of eccentricity were considered (values of eccentricity were determined by hole location within each specimen). A nonlinear finite element program was used for the analytical portion of this study. The nonlinear finite element analysis accounted for material nonlinearity only. To verify the predictions of the analytical study, experimentation was conducted. The effects of boundary conditions on the failure modes of the given laminates were examined through the use of a mounting fixture that allowed in-plane rotation of the specimens. Finally, photoelasticity was used to verify the "gross" states of strain predicted by the analytical study. There was good correlation between the analytical predictions of failure and the experimental data; however, for the $[\pm 45\ \text{deg}]_{4s}$ laminates, the analytical predictions were found to underestimate the experimental failure loads. The analytical study predicted that slightly lower failure loads would result from the use of the mounting fixture. Although limited testing was done using the mounting fixture, experimentation did verify slightly lower failure loads for the $[0\ \text{deg}_{16}]$ and $[0/\pm 45/90]_{2s}$ laminates when the mounting fixture was used. Finally, there was good correlation between the analytical predictions of the gross strain states and the actual strain states noted during photoelastic testing.**

## Introduction

IN weight-sensitive applications, such as aircraft design, accurate strength and failure characteristics must be ascertained before composite materials can be used to their full advantage. Therefore, future design advancements rely heavily upon our ability to accurately predict strength and failure characteristics of composite materials. This study attempted to further our understanding of the failure characteristics of Gr/PEEK laminates containing an eccentric 0.4-in.-diam circular discontinuity.[1]

The experimental and analytical objectives of this effort were as follows:

1) Investigate the initiation and progression of failure, and the failure loads of the Gr/PEEK laminates.

2) Investigate the boundary condition effects on the failure characteristics of the Gr/PEEK laminates.

3) Verify the analytical predictions of the "gross" strain states of the Gr/PEEK laminates.

4) Compare the experimental and analytical results.

## Analytical Studies

Since past research[2,3] has shown the stress-strain response of Gr/PEEK to be nonlinear, a nonlinear material finite element program was used in this study. This progressive-ply-failure program predicts both damage initiation and propagation in composite laminates.[4,5] The nonlinear material finite element program analyzes composite laminates on a ply-by-ply basis. In addition, the program takes into account the number and orientation of plies and specimen geometry. Failure of a laminate was determined by a total strain energy failure criterion.[4,5] For completeness, the failure criteria developed fully in Refs. 4 and 5 is briefly discussed here. This failure criterion is based on the concept that strain energies under longitudinal, transverse, and shear loadings are independent parameters. Therefore, the ratios of current energy levels (due to longitudinal, transverse, and shear loading) to the maximum energy levels that are available for each is considered by the failure criterion. If Eq. (1) is satisfied, lamina failure is assumed to have occurred:

$$K_1\left[\int_{\epsilon_1}\sigma_1 d\epsilon_1\right] + K_2\left[\int_{\epsilon_2}\sigma_2 d\epsilon_2\right] + K_6\left[\int_{\epsilon_6}\sigma_6 d\epsilon_6\right] = 1 \qquad (1)$$

where

$K_i$ = material characteristics (from stress-strain input data)
$\epsilon_i$ = strain components
$\sigma_i$ = stress components

From Fig. 1, note that the finite element model is refined near the discontinuity and near the tab area. This refinement was used in these areas since high gradients of stress were expected to result from both the discontinuity and the tabs. As a result of this mesh refinement, large jumps in stress were avoided as boundaries between finite elements were crossed.

Since a plane stress assumption was made in this study, each node of the finite-element model was allowed to have a maximum of two (in-plane) degrees of freedom ($x$ and $y$). Finally, since four different stacking sequences were considered in this study, it was necessary to model the various ply orientations through the thickness of the laminates. This through-the-thickness modeling of the ply orientations was necessary to

Received Feb. 2, 1990; revision received May 2, 1990; accepted for publication June 6, 1990. 

*Captain, United States Air Force; Graduate Student, School of Engineering; currently, Composites Structures Engineer, Structural Concepts Branch, Structures Division, Wright Research and Development Center, WPAFB, OH 45433. Member AIAA.

†Professor, Aeronautics and Astronautics, School of Engineering. Associate Fellow AIAA.

‡Aerospace Engineer, Structural Concepts Branch, Structures Division. Member AIAA.

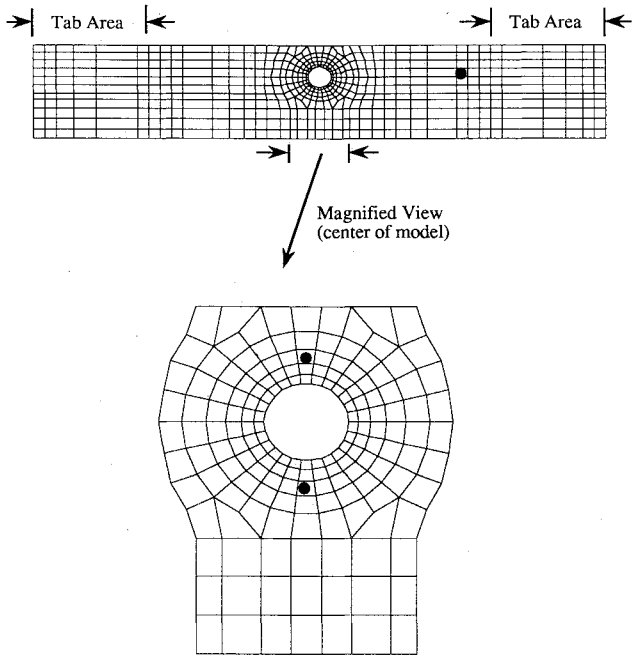


● indicates strain gage locations
NOTE: The gage near the tab area is mirrored by another strain gage on the reverse side of the specimen.

**Fig. 1 Strain-gauge locations (finite element model).**

formulate an equivalent stiffness matrix. The nonlinear finite element program makes use of the assumption that displacements through the thickness of the laminate are constant. Therefore, the equivalent stiffness matrix was formulated by summing up the individual stiffness matrices for each ply [see Eq. (2)].

$$[k_{eq}] = A \sum_{i=1}^{n} [B]^T [\bar{Q}_i][B] t_i \qquad (2)$$

where

$i$ = the $i$th lamina
$n$ = the total number of plies
$t_i$ = the thickness of the $i$th ply
$[B]$ = strain-displacement matrix
$[\bar{Q}_i]$ = transformed reduced stiffness matrix
$A$ = area

This through-the-thickness modeling of the ply orientations was accomplished by varying the number of through-the-thickness elements of each finite element model. The total number of elements for each stacking sequence was as follows: $[0\ \text{deg}_{16}]$: 831 elements; $[90\ \text{deg}_{16}]$: 831 elements; $[\pm 45\ \text{deg}]_{4s}$: 1142 elements; $[0/\pm 45/90]_{2s}$: 2664 elements.

This technique assumed a plane-stress condition (two-dimensional analysis) and did not consider interlaminar stresses. Since the specimens dealt with in this work were essentially thin plates, the plane-stress assumption was made. Therefore, the through-the-thickness normal stresses were neglected. Without this assumption, a three-dimensional finite element analysis would be required. Therefore, this study attempted to accurately model failure with a two-dimensional model.

The material property data for Gr/PEEK was entered into the nonlinear material program in the form of tabulated stress-strain data. This basic property data was obtained from tests conducted by Martin[2]; these tests and the resulting properties are shown in Table 1. Once the program read the tabulated stress-strain data, piecewise cubic spline interpolation functions were used to represent the data.

**Table 1 Property tests resulting curves/corresponding basic properties**

| Test | Curve | Property obtained |
|---|---|---|
| 0-deg tension | $\sigma_1$ vs $\epsilon_1$ | $E_1^T$ |
| | $\nu_{12}$ vs $\epsilon_1$ | $\nu_{12}^T$ |
| 0-deg compression | $\sigma_1$ vs $\epsilon_1$ | $E_1^C$ |
| | $\nu_{12}$ vs $\epsilon_1$ | $\nu_{12}^C$ |
| 90-deg tension | $\sigma_2$ vs $\epsilon_2$ | $E_2^T$ |
| 90-deg compression | $\sigma_2$ vs $\epsilon_2$ | $E_2^C$ |
| ±45-deg tension | $\tau_{12}$ vs $\gamma_{12}$ | $G_{12}$ |

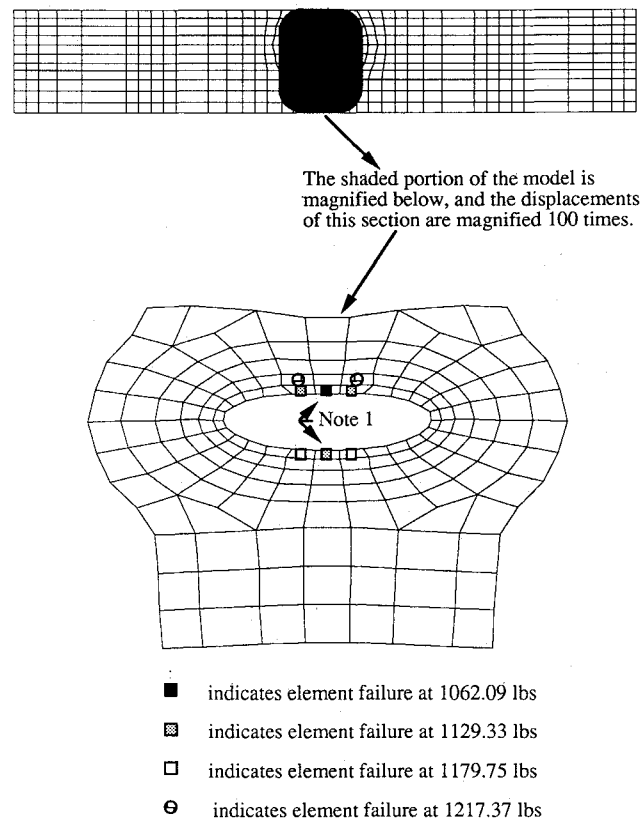


1. Free-floating nodes occurred (instability) @ 1179.75 lbs; in addition, the load increments converged at the FAILURE LOAD (1217.37 lbs).

**Fig. 2 Failure progression [90 deg$_{16}$] laminate (eccentricity = 0.3 in./no mounting fixture).**

The nonlinear material finite element program modeled the failure progression of the Gr/PEEK laminates as a damage accumulation process. This damage accumulation (failure progression) was modeled as areas of failure (finite element failures) within the finite element model. Figures 2–4 shows the analytical predictions of the damage accumulation process for each stacking sequence. From Figs. 2–4, note that there is no analytical predictions of damage accumulation for the [0 deg$_{16}$] laminates. This is because the [0 deg$_{16}$] laminates split along the fiber direction as soon as the ultimate strength of the laminate was reached (at the edge of the discontinuity). These splits are highlighted (by silver lines) on the failed [0 deg$_{16}$] specimens shown in Fig. 5.

Close inspection of Figs. 2–4 reveals that the eccentric circular discontinuity caused elements above the discontinuity to

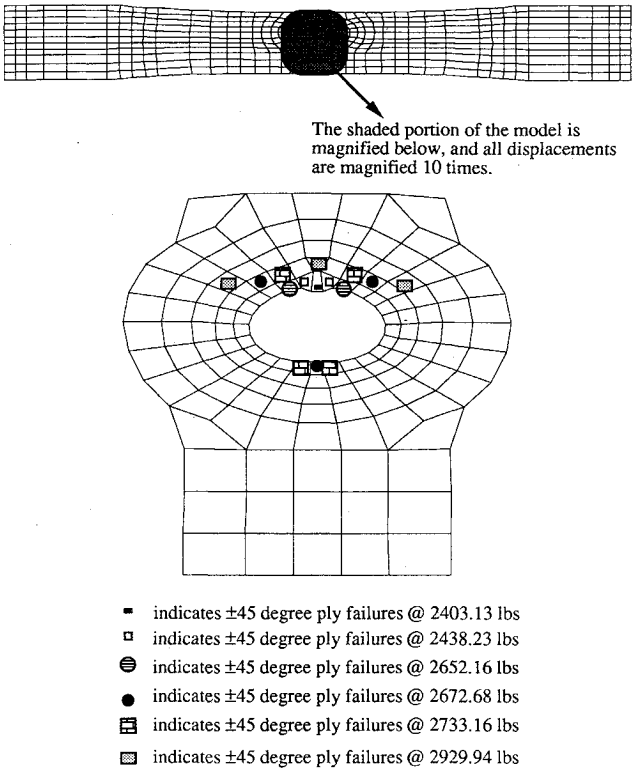


**Fig. 3 Failure progression $[\pm 45\ \text{deg}]_{4s}$ laminate (eccentricity = 0.3 in./no mounting fixture).**

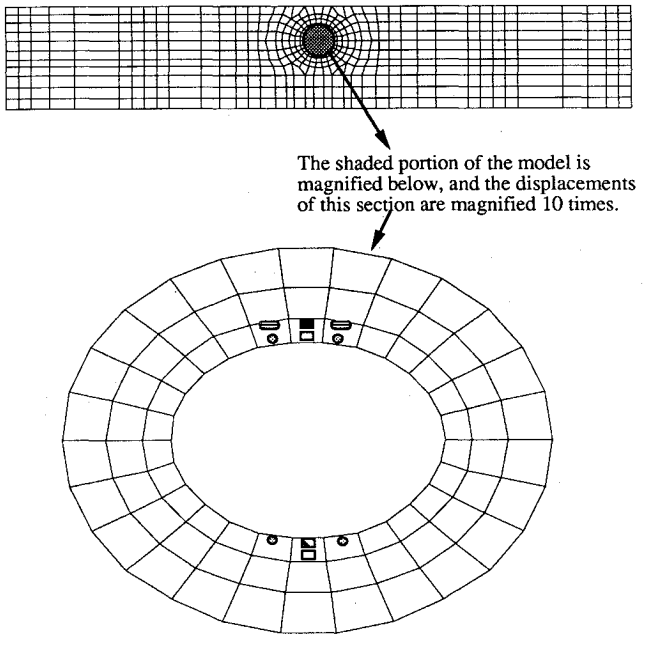


**Fig. 4 Failure progression $[0\ \text{deg}/\pm 45\ \text{deg}/90\ \text{deg}]_{2s}$ laminate (eccentricity = 0.3 in./no mounting fixture).**

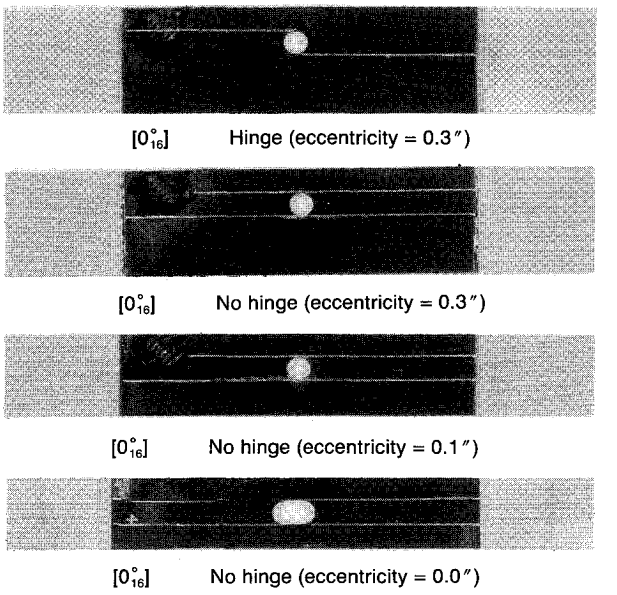


**Fig. 5 Failed specimens $[0\ \text{deg}_{16}]$ laminate.**

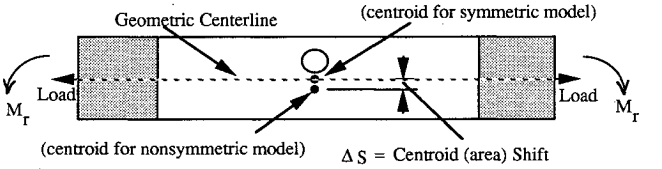


The eccentric circular discontinuity causes a centroid (area) shift. Therefore, the applied load (from the Instron) creates a bending moment ($M_r$ ).

$$M_r = \Delta S \times \text{Load}$$

**Fig. 6 Centroid shift and resulting bending moment.**

fail more quickly than corresponding elements below the discontinuity. This can be explained in terms of the centroid (area) shift caused by the eccentric circular discontinuity. This centroid shift (i.e., shift in area centroid) resulted in an in-plane bending moment that created higher tensile stresses above the discontinuity. The centroid shift and resulting bending moment are shown in Fig. 6.

## Experimentation

### Test Specimens

The Gr/PEEK specimens used in the experimental portion of this study were APC-2, and consisted of Hercules AS4 graphite fibers in a Victrex® PEEK matrix. The specimens were fabricated from 16-ply panels obtained from ICI Fiberite Corporation. The fiber content of these panels was 68% by weight. An ultrasonic inspection was conducted on all panels to ensure that they were free of significant defects.

Specimens were fabricated for each of the four stacking sequences. Specimen dimensions are depicted in Fig. 7.

### Specimen Instrumentation

A total of 48 specimens were instrumented with strain-gauge rosettes. These gauges (four per specimen) were bonded to the specimens as shown in Fig. 8. Stacked rosettes were used near the discontinuity (Fig. 8) since high strain gradients were expected at this location. As shown in Fig. 1, the strain gauges on each specimen were positioned with the center of each gauge located on the centroid of a single finite element. This placement was used because the nonlinear material finite element program gave stress and strain output data at the centroid of the finite elements. Therefore, no interpolation was required in the comparison of experimental and analytical data.

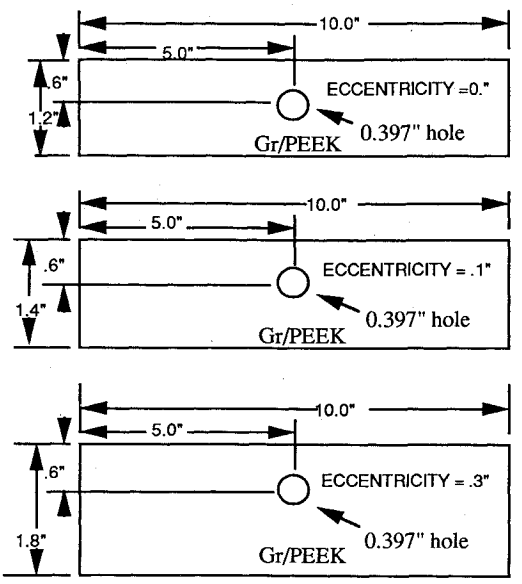


"top views" (tabs not shown on this view)

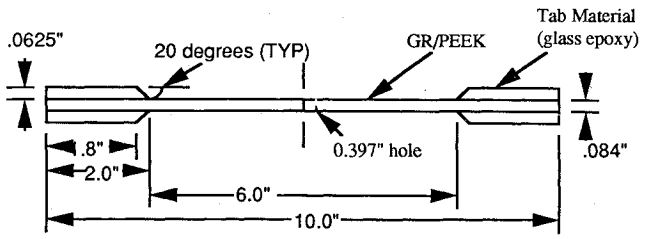


"side view"

**Fig. 7 Specimen geometry.**

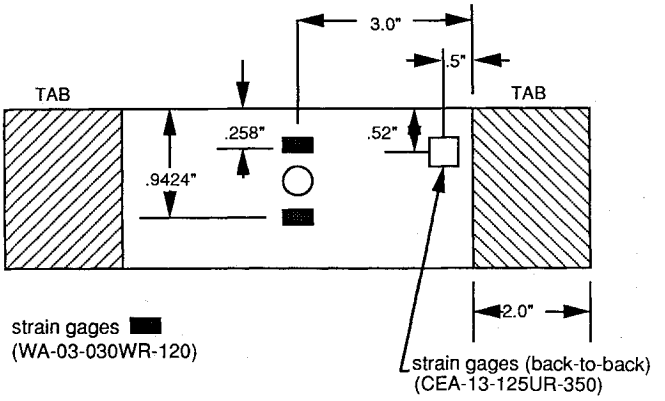


All strain gages manufacturered by Micro-Measurements

**Fig. 8 Strain-gauge locations.**

### Instrumented Specimen Testing

Of the 48 specimens instrumented with strain gauges, 36 were tested without the mounting fixture. The remaining 12 specimens were tested with the mounting fixture. This mounting fixture was based on a previous design used by Cron[6,7]; and, as mentioned previously, allowed the specimens to rotate in-plane (see Fig. 9). The mounting fixture was used to study the effects of boundary conditions on the failure characteristics of the Gr/PEEK laminates.

All 48 of the instrumented specimens were tested under a tensile load (until failure) using a 20-kip Instron Test Machine, Floor Model TT-1115. Testing was conducted at room temperature with a constant crosshead speed of 0.05 in./min. Of the 36 specimens tested without the mounting fixture, three specimens (for each stacking sequence) were tested for each of the three values of eccentricity shown in Fig. 7. For the 12 specimens tested with the mounting fixture, three specimens (for each stacking sequence) were tested for the 0.3-in. eccentricity specimens only (see Fig. 7).

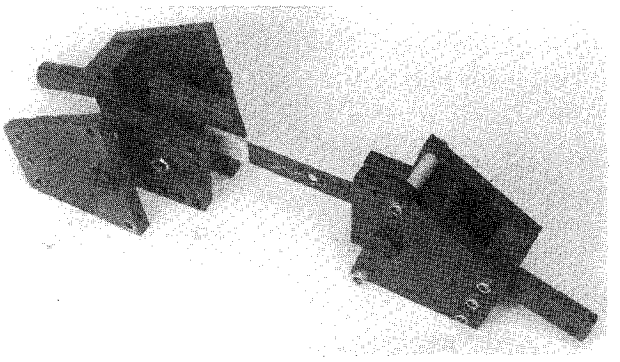

**Fig. 9 Mounting fixture.**

A video camera was used to provide a visual recording of all testing. A digital voltmeter was also used to provide load information at any given time. The voltmeter provided this load information by measuring the resistance across the load cell of the Instron Test Machine. Since all testing was recorded on video tape, the voltmeter (see Fig. 10) gave a visual indication of the applied load. This setup was ideal for postfailure analysis since specimen failure could be easily correlated with the failure load.

Typical failed specimens from this testing are shown in Figs. 5,11–13. The terms "hinge" and "no hinge" shown in Figs. 5,11–13 indicate whether the mounting fixture was or was not used, respectively.

Data from the strain gauges provided information from which stress-strain plots for each stacking sequence were constructed. Figures 14–17 show the experimental and analytical stress-strain response plots (discussed subsequently) for each stacking sequence. The analytical predictions of stress-strain response for each of the four stacking sequences are shown by a solid line (see Figs. 14–17). Also, from these figures, note that both the axial and transverse stress-strain response plots are shown for each stacking sequence. The experimental stress-strain data is depicted with symbols (Figs. 14–17) and this data is not connected with lines. The nonlinearity of the stress-strain response for Gr/PEEK is most noticeable in the plot for the $[\pm 45\ \text{deg}]_{4s}$ laminates (see Fig. 16). For the other stacking sequences, the nonlinear material behavior was not as pronounced.

Average experimental failure loads are compared to the analytical predictions in Tables 2–5. The percent difference shown in Tables 2–5 is relative to the average experimental failure loads. In addition, the standard deviation (not shown)

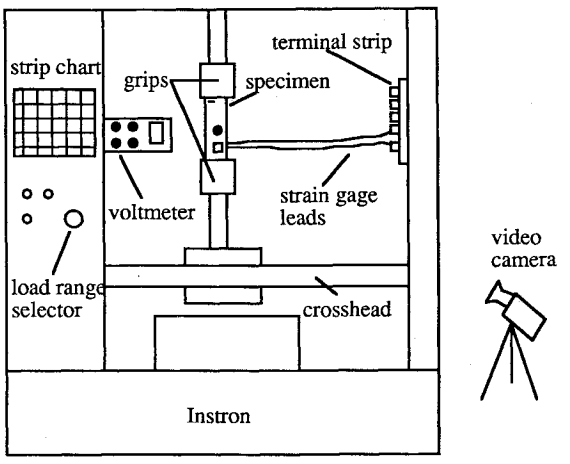


**Fig. 10 20-kip Instron Universal test machine.**

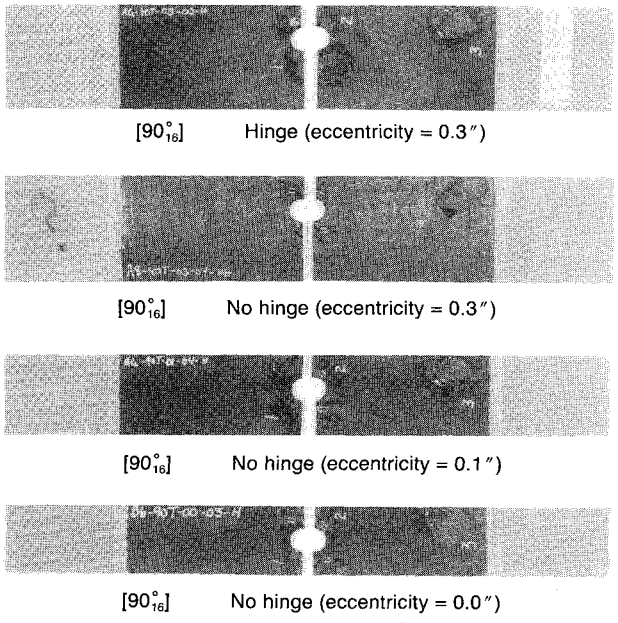


**Fig. 11 Failed specimens [90 deg$_{16}$] laminate.**

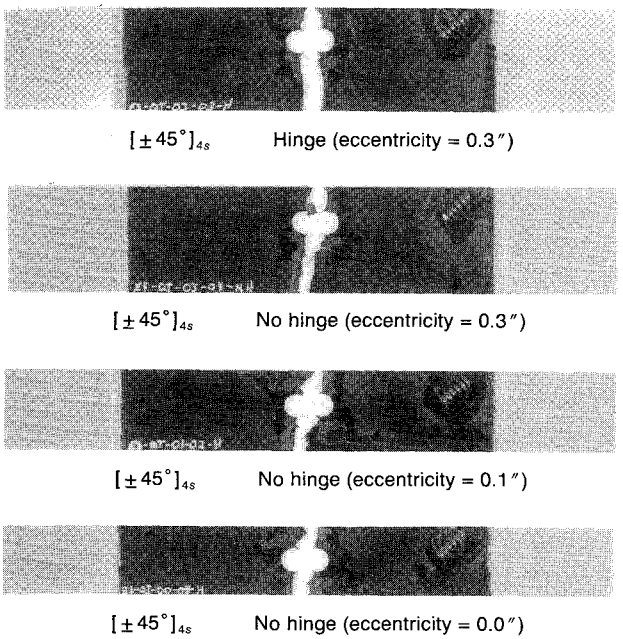


**Fig. 12 Failed specimens [±45 deg]$_{4s}$ laminate.**

for the experimental failure loads of each stacking sequence was calculated. The standard deviation was found to be acceptable for all stacking sequences, with a range no greater than 11% of the average experimental failure loads.

### Photoelastic Testing

Photoelasticity[8] was used to verify gross strain states predicted by the analytical study. For each stacking sequence, photoelastic coatings were applied to 0.0-in. eccentricity specimens. These specimens were then tested (without the mounting fixture) under tensile loading until failure. This testing was also conducted using the Instron Test Machine, at room temperature, with a constant crosshead speed of 0.05 in./min. Testing was recorded by video camera, and photographs were later obtained from the video tape at various levels of load. These photographs provided a mapping of the strain states of the specimens. Contour plots of the state of strain were constructed from analytical data and the photoelastic fringe pho-

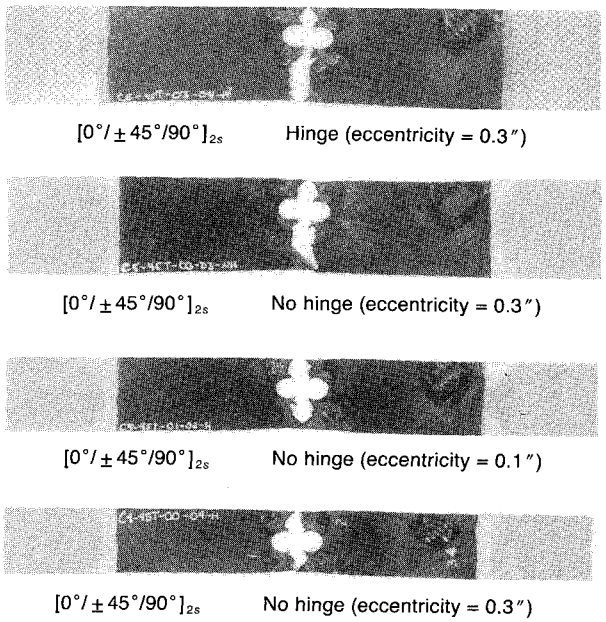


**Fig. 13 Failed specimens [0 deg/±45 deg/90 deg]$_{2s}$ laminate.**

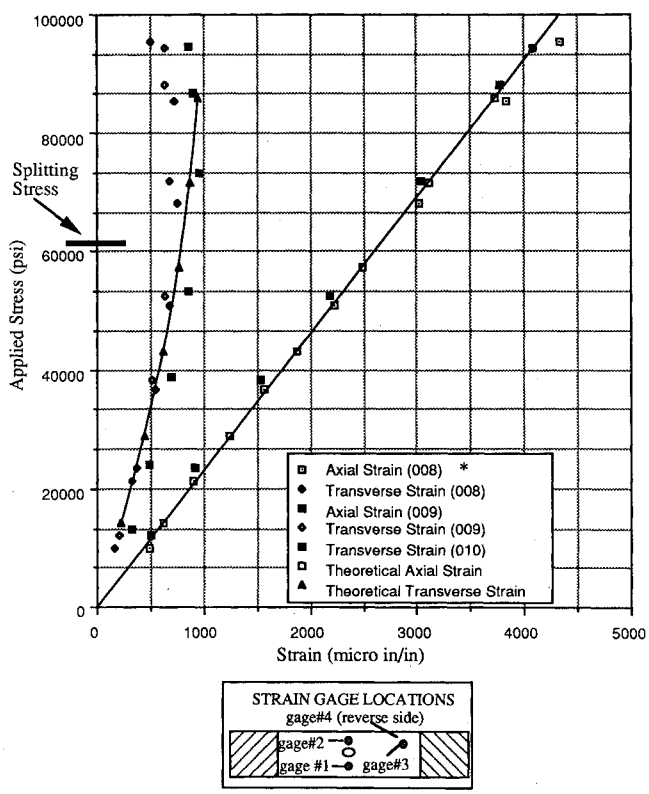


NOTES:

1. * indicates serial number of test specimen
2. axial strain for specimen #010 not available (bad gage)
3. 0 degree lay-up / eccentricity=0.3" / no mounting fixture

**Fig. 14 Stress-strain response (strain gauge no. 2) [0 deg$_{16}$] laminates.**

tographs were compared with the analytical contours. Figure 18 shows a comparison of the experimental and analytically obtained strain state "contours" for the [±45 deg]$_{4s}$ laminate loaded at 367.2 lb. Quantitative correlation between the experimental and analytically obtained strain states are shown in terms of the stress-strain response plots in Figs. 14–17. This quantitative correlation was only available at the four loca-

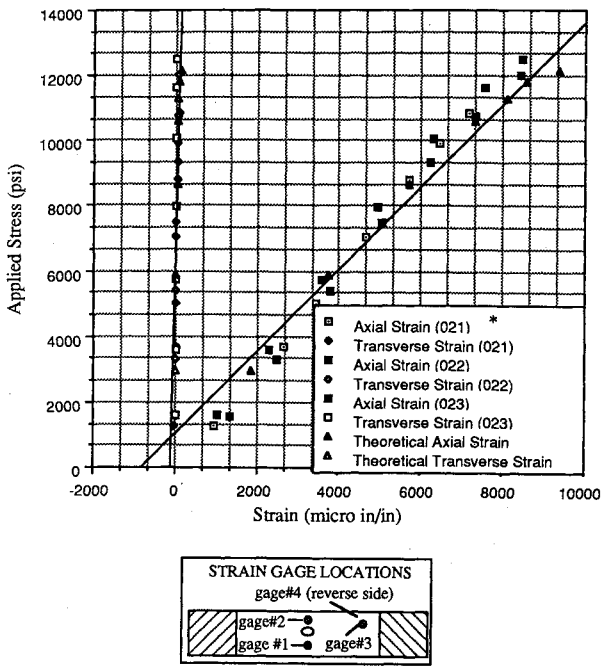


NOTES:

1. * indicates serial number of test specimen
2. 90 degree lay-up / eccentricity=0.3" / no mounting fixture

**Fig. 15 Stress-strain response (strain gauge no. 2) [90 deg$_{16}$] laminates.**

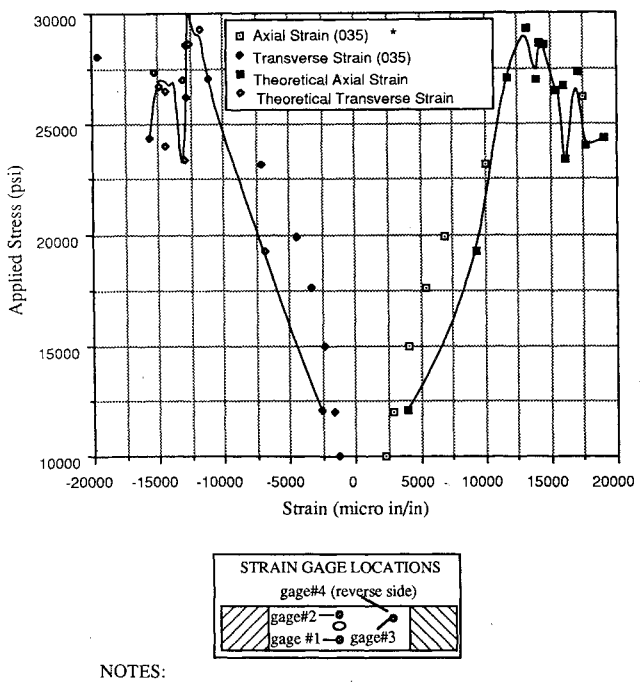


NOTES:

1. * indicates serial number of test specimen
2. ±45 degree lay-up / eccentricity=0.3" / no mounting fixture
3. no data available from specimens 034 & 036 (gages saturated)

**Fig. 16 Stress-strain response (strain gauge no. 2) [±45 deg]$_{4s}$ laminates.**

tions of the strain gauges (see Fig. 8 for strain gauge locations). Quantitative data was not obtainable from the photoelastic testing. However, the photoelastic "strain state" was

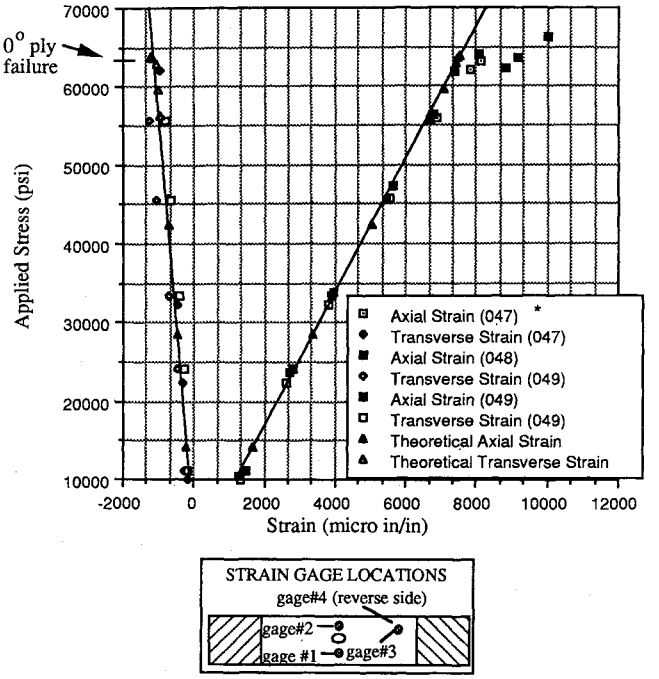


NOTES:

1. * indicates serial number of test specimen
2. quasi lay-up / eccentricity=0.3" / no mounting fixture

**Fig. 17 Stress-strain response (strain gauge no. 2) [0 deg/±45 deg/90 deg]$_{2s}$ laminates.**

**Table 2 Average experimental failure loads and analytical failure loads for [0 deg$_{16}$] laminates**

| Eccentricity | Average experimental failure load, lb | Analytical failure load, lb | % difference (experimental vs analytical) |
|---|---|---|---|
| 0.0 in. (no fixture) | 5156.41 | 5935.36 | −15.1 |
| 0.1 in. (no fixture) | 6917.92 | 7041.71 | −1.8 |
| 0.3 in. (no fixture) | 9478.44 | 9241.27 | +2.5 |
| 0.3 in. (with fixture) | 8138.86 | 8952.14 | −9.1 |

**Table 3 Average experimental failure loads and analytical failure loads for [90 deg$_{16}$] laminates**

| Eccentricity | Average experimental failure load, lb | Analytical failure load, lb | % difference (experimental vs analytical) |
|---|---|---|---|
| 0.0 in. (no fixture) | 748.82 | 729.05 | +2.6 |
| 0.1 in. (no fixture) | 876.84 | 894.89 | −2.1 |
| 0.3 in. (no fixture) | 1177.17 | 1217.37 | −3.4 |
| 0.3 in. (with fixture) | 1221.70 | 1172.56 | +4.0 |

used only to verify the gross strain-state predictions of the finite element model.

## Discussion of Results and Conclusions

### [0 deg$_{16}$] Laminates

The finite element (FE) solution predicted the splitting (failure) loads for these laminates. In addition, the FE stress-strain

**Table 4 Average experimental failure loads and analytical failure loads for $[\pm 45\ \text{deg}]_{4s}$ laminates**

| Eccentricity | Average experimental failure load, lb | Analytical failure load, lb | % difference (experimental vs analytical) |
|---|---|---|---|
| 0.0 in. (no fixture) | 2338.08 | 1949.26 | +16.6 |
| 0.1 in. (no fixture) | 3037.64 | 2133.70 | +29.8 |
| 0.3 in. (no fixture) | 3988.93 | 2931.39 | +26.5 |
| 0.3 in. (with fixture) | 4354.61 | 2590.33 | +40.5 |

**Table 5 Average experimental failure loads and analytical failure loads for $[0\ \text{deg} \pm 45\ \text{deg}/90\ \text{deg}]_{2s}$ laminates**

| Eccentricity | Average experimental failure load, lb | Analytical failure load, lb | % difference (experimental vs analytical) |
|---|---|---|---|
| 0.0 in. (no fixture) | 4067.90 | 3920.27 | +3.6 |
| 0.1 in. (no fixture) | 5041.56 | 4810.02 | +4.6 |
| 0.3 in. (no fixture) | 6683.89 | 6388.39 | +4.4 |
| 0.3 in. (with fixture) | 6451.95 | 6323.25 | +2.0 |

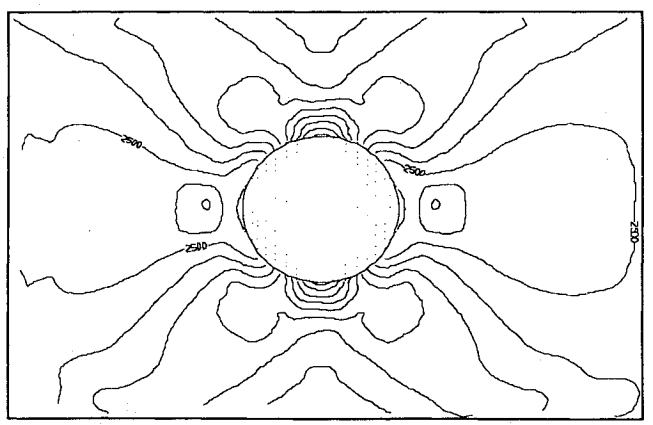


applied loading=367.2 lbs / contour plot

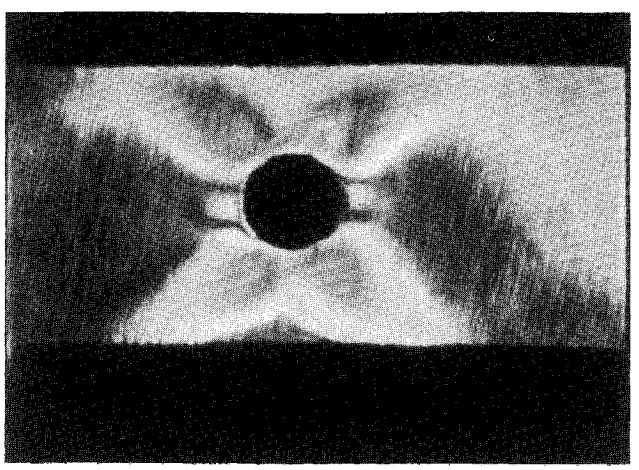

**Fig. 18 Analytical vs experimental contours ($[\pm 45\ \text{deg}]_{4s}$ laminate).**

response predictions correlated well with the experimental stress-strain response. However, the FE solution did not predict the failure progression (i.e., splitting) in terms of damage accumulation. The splitting of these laminates may be caused by a dynamic phenomenon, such as a stress wave. The splitting phenomenon occurred so rapidly that it was not observable by viewing the video tape frame-by-frame (frame-by-frame viewing did not allow events that occurred in less than 1 s to be observed). In addition, there may be some three-dimensional effects, such as edge effects, which affect the failure characteristics of these laminates. Therefore, the two-dimensional FE solution was not able to predict failure progression.

#### $[90\ \text{deg}_{16}]$ Laminates

For these laminates, the FE solution correlated very well with the experimental failure loads and the experimental stress-strain response. In addition, the numerical predictions of damage accumulation (failure progression) showed that damage initiation would occur above and below the discontinuity, and that failure would occur rapidly once the damage initiation occurred. These predictions (of failure progression) matched the results obtained from experimentation, where it was observed that these laminates failed suddenly, and damage initiation occurred above and below the discontinuity.

#### $[\pm 45\ \text{deg}]_{4s}$ Laminates

For these laminates, the FE solution was found to significantly underestimate the experimental failure loads. This underestimation may be due to geometric nonlinearities observed during the experimentation, or may be a result of ignoring the interlaminar stresses (since this was a two-dimensional study). The experimental scattering of test data was not significant enough to account for the numerical underestimation of the failure loads.

The FE solution predicted the high strains (necking) at failure. Finally, although the FE predictions of stress-strain response correlated, for low levels of load, with the experimental stress-strain response, the experimentation did not provide enough useful data to verify the analytical predictions of the stress-strain response.

#### $[0\ \text{deg}/\pm 45\ \text{deg}/90\ \text{deg}]_{2s}$ Laminates

The FE solution predicted the experimental failure loads for these laminates. In addition, the FE stress-strain response predictions, up to the point of failure, correlated well with the experimental stress-strain response.

The failure of these laminates was characterized by a shear failure. However, the failure regions of these laminates did not appear to be as shear dominated as was noted for the $[45\ \text{deg}]_{4s}$ laminates. Therefore, it appears that the failure mode for these laminates is some combination of the failure modes noted for the $[0\ \text{deg}_{16}]$, $[90\ \text{deg}_{16}]$, and $[45\ \text{deg}]_{4s}$ laminates.

The FE solution did not predict the shear failure. This may be due to several reasons. First, the $\pm 45$-deg plies require large strains before failure; but, the 0-deg plies in the $[0\ \text{deg}/\pm 45\ \text{deg}/90\ \text{deg}]_{2s}$ laminate prevent large strains. Therefore, once the level of loading was high enough to cause failure of the 0-deg plies, adjacent (above and below) to the discontinuity, the level of load was much higher than the neighboring $\pm 45$-deg plies (or 90-deg plies) could sustain. As a result, the FE solution predicted catastrophic failure of these laminates once the 0-deg plies, adjacent (above and below) to the discontinuity, failed. Another possibility that might have affected the FE predictions of damage progression is the fact that the two-dimensional FE solution did not account for interlaminar stresses, which for this stacking sequence, may alter the failure mode.

During the experimentation, audible "popping" of the fibers could be heard for several minutes before the laminates failed. Therefore, one would think that the damage zone (at

the failure load) would not be as small as the damage zone predicted by the FE solution (see Fig. 4). One possibility for the prediction of a small damage zone is the fact that interlaminar stresses were ignored in this study, and as mentioned previously, these stresses may have an effect on the failure characteristics of this stacking sequence.

#### Boundary-Condition Effects

The nonlinear FE study predicted that lower (within a range no greater than 13%) failure loads would result from the use of the mounting fixture.[1] These lower failure loads appear to result from the in-plane rotation allowed by the mounting fixture. This in-plane rotation results in a higher axial stress region above the discontinuity, and consequently led to failure at lower levels of load.

The experimental verification of the FE predictions of boundary-condition effects was inconclusive. Since only three specimens (for each stacking sequence and value of eccentricity) were tested experimentally, experimental scattering of test data could account for not always observing a lowering of the experimental failure loads through the use of the mounting fixture. It should be noted that the experimentation did verify lower failure loads for the $[0\ \text{deg}_{16}]$ and $[0\ \text{deg}/\pm 45\ \text{deg}/90\ \text{deg}]_{2s}$ laminates when the mounting fixture was used.

#### Eccentricity Effects

The eccentric circular discontinuity created a centroid (area) shift. This centroid shift, and resulting bending moment, created higher tensile stresses above the discontinuity. This phenomenon was predicted by the FE study, and it was observed that elements above the discontinuity tended to fail more quickly than corresponding elements below the discontinuity. Therefore, eccentricity effects led to a higher axial stress region above the discontinuity. However, the nominal (far-field) failure stresses, for all four stacking sequences, did not vary by more than 13% for the different values of eccentricity considered.

Eccentricity effects (in terms of failure progression) were not observed experimentally. This was because failure was too rapid to determine if (by viewing a video tape of the testing frame-by-frame) failure initiated above or below the discontinuity. Future work required to verify eccentricity effects should include specimens that have been tested to a percentage of their ultimate load. These specimens should then be examined using stereo x-ray techniques[2,3] to provide further insight into the eccentricity effects on the initiation and progression of failure.

## References

[1]Daniels, J. A., "A Study of Failure Characteristics in Thermoplastic Composite Laminates Due to an Eccentric Circular Discontinuity," M.S. Thesis, School of Engineering, Air Force Inst. of Technology (AU), Wright-Patterson AFB, OH, AFIT/GAE/AA/89D-06, Dec. 1989.

[2]Martin, J., "A Study of Failure Characteristics in Thermoplastic Composite Material," M.S. Thesis, School of Engineering, Air Force Inst. of Technology (AU), Wright-Patterson AFB, OH, AFIT/GA/AA/88M-2, March 1988.

[3]Fisher, J. M., "A Study of Failure Characteristics in a Thermoplastic Composite Material at High Temperature," M.S. Thesis, School of Engineering, Air Force Inst. of Technology (AU), Wright-Patterson AFB, OH, AFIT/GAE/AA/88D-15, Dec. 1988.

[4]Sandhu, R. S. "Nonlinear Behavior of Unidirectional and Angle Ply Laminates," *Journal of Aircraft,* Vol. 13, Feb. 1976, pp. 104–111.

[5]Sandhu, R. S., "Ultimate Strength Analysis of Symmetric Laminates," Air Force Flight Dynamics Lab., Wright-Patterson AFB, OH, AFFDL-TR- 73-137, AD 779927, Feb. 1974.

[6]Cron, S. M., "Improvement of End Boundary Conditions for Off-Axis Tension Specimen Use," M.S. Thesis, School of Engineering, Air Force Inst. of Technology (AU), Wright-Patterson AFB, OH, AFIT/GAE/AA/85D-3, Dec. 1985.

[7]Cron, S. M., Palazotto, A. N., and Sandhu, R. S., "Improvement of End Boundary Conditions for Off-Axis Tension Specimen Use," *Experimental Mechanics,* Vol. 28, No. 1, 1988, pp.14–19.

[8]*Introduction to Stress Analysis by the Photoelastic Coating Technique,* Technical Bulletin TDG-1, Photoelastic, Inc., Malvern, PA, 1974.